

Constraining models with a large scalar multiplet

Kevin Earl,^{*} Katy Hartling^{b,‡} Heather E. Logan,[§] and Terry Pilkington[¶]

Ottawa-Carleton Institute for Physics, Carleton University, Ottawa, Ontario K1S 5B6, Canada

(Dated: March 5, 2013)

Models in which the Higgs sector is extended by a single electroweak scalar multiplet X can possess an accidental global $U(1)$ symmetry at the renormalizable level if X has isospin $T \geq 2$. We show that all such models with an accidental $U(1)$ symmetry are excluded by the interplay of the cosmological relic density of the lightest (neutral) component of X and its direct-detection cross section via Z exchange. The sole exception is the $T = 2$ multiplet, whose lightest member decays on a few-day to few-year time scale via a Planck-suppressed dimension-5 operator.

^b Formerly Katy Hally.

^{*} kevinearl@gmail.carleton.ca

[‡] khally@physics.carleton.ca

[§] logan@physics.carleton.ca

[¶] tpilking@physics.carleton.ca

I. INTRODUCTION

Extensions of the scalar sector of the Standard Model (SM) beyond the minimal single Higgs doublet are of great interest in model building and collider phenomenology and are, as yet, largely unconstrained by experiment. Such extensions are common in models that address the hierarchy problem of the SM, such as supersymmetric models [1] and little Higgs models [2], as well as in models for neutrino masses, dark matter, etc. Most of these extensions contain additional $SU(2)_L$ -singlet, -doublet, and/or -triplet scalar fields. However, some extensions of the SM contain scalars in larger multiplets of $SU(2)_L$. Such larger multiplets have been used to produce a natural dark matter candidate [3–5], which is kept stable thanks to an accidental global symmetry present in the Higgs potential for multiplets with isospin $T \geq 2$. Three different models with a Higgs quadruplet ($T = 3/2$) have also been proposed for neutrino mass generation [6–8]. Models in which the SM $SU(2)$ -doublet Higgs mixes with a seven-plet ($T = 3$), aided by additional representations of $SU(2)$, have also been studied recently in Ref. [9].

In this paper we consider models that extend the SM scalar sector through the addition of a *single* large multiplet. For multiplets with $n \equiv 2T + 1 \geq 5$ (isospin 2 and larger), the scalar potential of these models always preserves an accidental global $U(1)$ or Z_2 symmetry at the renormalizable level. If unbroken, such a symmetry forces the lightest member of the large multiplet to be stable. Spontaneous breaking of an accidental global $U(1)$ symmetry is phenomenologically unacceptable because it would lead to a massless Goldstone boson that couples to fermions through its mixing with the SM Higgs doublet’s neutral Goldstone, and thus mediate new long-range forces between SM fermions. Furthermore, perturbative unitarity of scattering amplitudes involving pairs of scalars and pairs of $SU(2)$ gauge bosons requires that $T \leq 7/2$ (i.e., $n \leq 8$) for a complex scalar multiplet and $T \leq 4$ (i.e., $n \leq 9$) for a real scalar multiplet [10].

The models that preserve such an accidental global symmetry can be grouped into three classes based on the hypercharge Y of the large multiplet, as follows:

- (i) Models with a $Y = 0$ multiplet, with $n = 5, 7$, or 9 , corresponding to isospin 2, 3, or 4.¹ In the most general case the large multiplet is odd under an accidental global Z_2 symmetry; though an additional $U(1)$ symmetry may be imposed by hand [11], it will not be accidental. These models have previously been considered in Refs. [3, 4] as possible candidates for “next-to-minimal” dark matter.
- (ii) Models with a complex multiplet with $n = 5, 6, 7$, or 8 , with $Y = 2T$ (we work in the convention $Q = T^3 + Y/2$). The large multiplet is charged under an accidental global $U(1)$ symmetry. The hypercharge is chosen so that the lightest member of the multiplet can be electrically neutral.² The masses of the states in the large multiplet are split by an operator of the form $(\Phi^\dagger \tau^a \Phi)(X^\dagger T^a X)$, where Φ is the SM Higgs doublet, X is the large multiplet, and τ^a and T^a are the appropriate $SU(2)$ generators. We study these models in the current paper.
- (iii) Models with a complex multiplet with $n = 6$ or 8 , with $Y = 1$. The large multiplet is odd under an accidental global Z_2 symmetry. The would-be accidental global $U(1)$ symmetry is broken by an operator of the form $(\Phi^\dagger \tau^a \tilde{\Phi})(\tilde{X}^\dagger T^a X)$, where $\tilde{\Phi}$, \tilde{X} denote the conjugate

¹ Note that a real multiplet must have integer isospin, and a complex $Y = 0$ multiplet can always be written in terms of two real $Y = 0$ multiplets.

² Models in which the lightest member of the large multiplet is electrically charged are excluded or strongly constrained by the absence of electrically charged relics. Metastable multicharged states are constrained by direct collider searches to be heavier than about 400–500 GeV, depending on their charge [12].

multiplets. Such an operator can appear only when n is even. We will address these models in a forthcoming paper [13].

In this paper we study the constraints on the models with a complex multiplet with $n = 5, 6, 7$, or 8 and $Y = 2T$. We first determine the constraints on the scalar quartic couplings from perturbative unitarity and precision electroweak measurements. We then examine the bounds on the neutral scalar χ^0 from cosmological considerations. Our goal is not to determine whether χ^0 is able to account for the entire observed quantity of dark matter—this possibility is strongly excluded by dark matter direct-detection experiments—but rather to evaluate the ultimate viability of the model as a target for collider searches. Assuming a standard thermal history of the universe, we compute the thermal relic density of χ^0 and χ^{0*} and compare it with the limits from dark matter direct-detection experiments. In conjunction with the requirement that $m_{\chi^0} \gtrsim m_Z/2 \simeq 45$ GeV from the invisible width of the Z boson, we find that these cosmological constraints exclude the models with $n = 6, 7$, and 8 .

The $n = 5$ ($T = 2$) multiplet has a dimension-5 Planck-suppressed interaction with the SM Higgs doublet of the form

$$\mathcal{L} \supset \frac{1}{M_{Pl}} \Phi \Phi \Phi X^\dagger + \text{h.c.}, \quad (1)$$

where M_{Pl} is the Planck mass. This operator induces a mixing of the SM Higgs into the neutral component of X , $\chi' = \chi^{0,r} - \epsilon \phi^{0,r}$, with $\epsilon \sim v^3 / [(m_{\chi^0}^2 - m_h^2) M_{Pl}]$. Here $v \simeq 246$ GeV is the SM Higgs vacuum expectation value. The neutral member of X can then decay via its Higgs component. Assuming that χ^0 is the lightest state, its lifetime ranges from a few days to a few years for $m_{\chi^0} \sim 100$ – 1000 GeV. This puts the decays of the lightest neutral state of the $n = 5$ model well after big-bang nucleosynthesis and well before the recombination surface of the cosmic microwave background radiation. Direct detection constraints from present-day experiments therefore do not apply to this model, and it remains viable [11].

The paper is organized as follows. In Sec. II we give the Lagrangians and mass spectra for the four models that we consider. In Sec. III we obtain the indirect constraints on the model parameters from unitarity and the oblique parameters, and comment on collider constraints. In Sec. IV we calculate the upper bound on the relic density of neutral scalars χ^0, χ^{0*} from dark matter direct-detection experiments. In Sec. V we compute the relic density from thermal freeze-out and show that in all cases it yields a relic density too large to be consistent with the bound from direct detection. We conclude in Sec. VI. Feynman rules, formulas for the oblique parameters, and formulas for the partial decay width of the SM Higgs to two photons are collected in the appendices.

II. THE MODELS

The models that we consider extend the SM through the addition of a single complex scalar multiplet X , with hypercharge $Y = 2T$ (normalized so that $Q = T^3 + Y/2$). The hypercharge is chosen so that the lightest member of X can be neutral. The size of the multiplet X is restricted to $n \equiv 2T + 1 \leq 8$ by the requirement that tree-level amplitudes for $SU(2)$ gauge bosons scattering into the states in X , $W^a W^a \rightarrow \chi^{Q*} \chi^Q$, remain perturbative [10]. When $n \geq 5$, the scalar potential possesses an accidental global $U(1)$ symmetry corresponding to phase rotations of X . This $U(1)$ symmetry ensures that the lightest member of X is stable, at least at the level of renormalizable operators. These two conditions leave us with four models to consider, with $n = 5, 6, 7$, and 8 .

The gauge-invariant scalar potential is given by

$$V(\Phi, X) = m^2 \Phi^\dagger \Phi + M^2 X^\dagger X + \lambda_1 (\Phi^\dagger \Phi)^2 + \lambda_2 \Phi^\dagger \Phi X^\dagger X + \lambda_3 \Phi^\dagger \tau^a \Phi X^\dagger T^a X + \mathcal{O}(X^4), \quad (2)$$

where τ^a and T^a are the generators of $SU(2)_L$ in the doublet and n -plet representations, respectively, Φ is the usual SM Higgs doublet, and the large scalar multiplet takes the form

$$X = (\chi^{+(n-1)}, \dots, \chi^0)^T. \quad (3)$$

The mass of particle χ^Q with charge $Q = T^3 + Y/2 \geq 0$ is given by

$$m_{\chi^Q}^2 = M^2 + \frac{1}{2}v^2 \left[\lambda_2 - \frac{1}{2}\lambda_3 T^3 \right] = M^2 + \frac{1}{2}v^2 \left[\lambda_2 - \frac{1}{2}\lambda_3 \left(Q - \frac{n-1}{2} \right) \right] \equiv M^2 + \frac{1}{2}v^2 \Lambda_Q, \quad (4)$$

where $v \simeq 246$ GeV is the SM Higgs vacuum expectation value (vev) and we define the dimensionless couplings Λ_Q as the quantity in square brackets above. The neutral particle χ^0 , with $T^3 = -T = -(n-1)/2$, will have a mass,

$$m_{\chi^0}^2 = M^2 + \frac{1}{2}v^2 \left[\lambda_2 + \frac{1}{4}\lambda_3(n-1) \right] = M^2 + \frac{1}{2}v^2 \Lambda_0. \quad (5)$$

The masses of the charged states χ^Q can be written in terms of the χ^0 mass as

$$m_{\chi^Q}^2 = m_{\chi^0}^2 - \frac{1}{4}v^2 \lambda_3 Q. \quad (6)$$

We require that the stable lightest member of X is electrically neutral; this forces us to take $\lambda_3 < 0$.

III. CONSTRAINTS ON COUPLINGS AND MASSES

A. Unitarity constraints on scalar quartic couplings

The scalar quartic couplings λ_2 and λ_3 given in Eq. (2) can be bounded by requiring perturbative unitarity of the zeroth partial wave amplitude. The partial wave amplitudes are related to scattering matrix elements according to

$$\mathcal{M} = 16\pi \sum_J (2J+1) a_J P_J(\cos \theta), \quad (7)$$

where J is the orbital angular momentum of the final state and $P_J(\cos \theta)$ is the corresponding Legendre polynomial. Perturbative unitarity of the zeroth partial wave amplitude dictates the tree-level constraint,

$$|\text{Re } a_0| \leq \frac{1}{2}. \quad (8)$$

The coupling λ_2 controls the strength of the isospin-zero $\chi^* \chi \rightarrow \phi^* \phi$ amplitude, while λ_3 controls the strength of the isospin-one $\chi^* \chi \rightarrow \phi^* \phi$ channel. Because we are working with large scalar

multiplets, the isospin-zero $\chi^*\chi \rightarrow WW, BB$ and isospin-one $\chi^*\chi \rightarrow WB$ amplitudes can be significant [10], leading to more stringent coupled-channel limits on λ_2 and λ_3 . We neglect all other contributing processes³ and work in the high-energy limit.

The relevant amplitudes for the isospin-zero channels are

$$\begin{aligned} a_0([\chi^*\chi]_0 \rightarrow [\phi^*\phi]_0) &= -\frac{\sqrt{n}}{8\sqrt{2}\pi}\lambda_2, \\ a_0([\chi^*\chi]_0 \rightarrow [WW]_0) &= \frac{g^2}{16\pi} \frac{(n^2-1)\sqrt{n}}{2\sqrt{3}}, \\ a_0([\chi^*\chi]_0 \rightarrow [BB]_0) &= \frac{g^2}{16\pi} \frac{s_W^2}{c_W^2} \frac{Y^2\sqrt{n}}{2} = \frac{g^2}{16\pi} \frac{s_W^2}{c_W^2} \frac{(n-1)^2\sqrt{n}}{2}, \end{aligned} \quad (9)$$

where the $\chi^*\chi \rightarrow WW, BB$ amplitudes include both of the contributing transverse gauge boson polarization combinations [10] and we used $Y = 2T = n-1$ in the last line. Here g is the $SU(2)_L$ gauge coupling and $s_W, c_W \equiv \sin\theta_W, \cos\theta_W$ are the sine and cosine of the weak mixing angle. We define the following normalized isospin-zero field combinations,

$$\begin{aligned} [\phi^*\phi]_0 &= \frac{1}{\sqrt{2}}(\phi^+\phi^- + \phi^{0*}\phi^0), \\ [\chi^*\chi]_0 &= \frac{1}{\sqrt{n}} \sum_{Q=0}^{n-1} \chi^{Q*}\chi^Q, \\ [WW]_0 &= \frac{1}{\sqrt{3}} \left(\sqrt{2}W^+W^- + \left(\frac{W^3W^3}{\sqrt{2}} \right) \right), \\ [BB]_0 &= BB/\sqrt{2}. \end{aligned} \quad (10)$$

The relevant amplitudes for the isospin-one channels are

$$\begin{aligned} a_0([\chi^*\chi]_1 \rightarrow [\phi^*\phi]_1) &= -\frac{\sqrt{n(n^2-1)}}{32\sqrt{6}\pi}\lambda_3, \\ a_0([\chi^*\chi]_1 \rightarrow [WB]_1) &= \frac{g^2}{16\pi} \frac{s_W}{c_W} \frac{Y\sqrt{n(n^2-1)}}{\sqrt{6}} = \frac{g^2}{16\pi} \frac{s_W}{c_W} \frac{(n-1)\sqrt{n(n^2-1)}}{\sqrt{6}}, \end{aligned} \quad (11)$$

where again the $\chi^*\chi \rightarrow WB$ amplitude includes both of the contributing transverse gauge boson polarization combinations [10]. Here we used the following normalized isospin-one field combinations,

$$\begin{aligned} [\phi^*\phi]_1 &= \frac{1}{\sqrt{2}}(\phi^+\phi^- - \phi^{0*}\phi^0), \\ [\chi^*\chi]_1 &= \sqrt{\frac{12}{n(n^2-1)}} \sum_{Q=0}^{n-1} \chi^{Q*}T^3\chi^Q = \sqrt{\frac{12}{n(n^2-1)}} \sum_{Q=0}^{n-1} \chi^{Q*} \left[Q - \frac{n-1}{2} \right] \chi^Q, \\ [WB]_1 &= W^3B. \end{aligned} \quad (12)$$

³ Additional contributions to the matrix of coupled-channel amplitudes come from quartic couplings of X as well as $\phi^*\phi \rightarrow \phi^*\phi$ amplitudes proportional to λ_1 . We find numerically that including these contributions generically leads to a slightly tighter constraint on λ_2 and λ_3 , but this constraint depends on the interplay between the λ_1 contributions and those from the quartic X couplings.

n	$ \lambda_2^{\text{lim}} $	$ \lambda_3^{\text{lim}} $
5	7.64	11.1
6	6.49	8.17
7	5.01	6.11
8	2.17	4.41

TABLE I. Upper limits on $|\lambda_2|$ and $|\lambda_3|$ from perturbative unitarity, for $Y = 2T = n - 1$.

Finding the largest eigenvalue of each coupled-channel matrix and applying the unitarity constraint of Eq. (8), we find the unitarity bounds on λ_2 and λ_3 ,

$$\begin{aligned}
|\lambda_2| &\leq \sqrt{\frac{32\pi^2}{n} - g^4 \frac{(n^2 - 1)^2}{24} - g^4 \frac{s_W^4}{c_W^4} \frac{(n - 1)^4}{8}}, \\
|\lambda_3| &\leq 2\sqrt{\frac{384\pi^2}{n(n^2 - 1)} - g^4 \frac{s_W^2}{c_W^2} (n - 1)^2}.
\end{aligned} \tag{13}$$

Recall that λ_3 must be negative so that χ^0 is the lightest member of the large multiplet. λ_2 can have either sign. Numerical bounds are given for $n = 5, 6, 7$, and 8 in Table I.⁴

B. Electroweak precision constraints

The multiplet X contributes to electroweak observables through the oblique parameters S , T , and U [14]. The contributions of such a scalar multiplet obeying a $U(1)$ global symmetry, so that the mass eigenstates have definite T^3 , were computed for arbitrary isospin and hypercharge in Ref. [15]. We summarize the results in Appendix B for completeness.

The contributions to the oblique parameters depend only on n , Y , and the masses m_{χ^Q} of each state in the multiplet. Therefore, for a given n and setting $Y = 2T = n - 1$, the oblique parameters constrain only two model parameters, which can be chosen as m_{χ^0} (which sets the overall mass scale) and λ_3 (which controls the mass splittings).

The current experimental values relative to the SM with Higgs mass $m_h = 126$ GeV are $S_{\text{exp}} = 0.03 \pm 0.10$, $T_{\text{exp}} = 0.05 \pm 0.12$, $U_{\text{exp}} = 0.03 \pm 0.10$, with relative correlations of $\rho_{ST} = 0.89$, $\rho_{TU} = -0.83$, $\rho_{SU} = -0.54$ [16]. We use these values to constrain m_{χ^0} and λ_3 via a two-parameter χ^2 variable; for details see Appendix B. We show 95% confidence level ($\chi^2 = 5.99$) limits for the two parameters m_{χ^0} and $\Delta m \equiv m_{\chi^+} - m_{\chi^0}$ in Fig. 1.

At low m_{χ^0} the constraint is dominated by the S parameter and leads to an upper bound on Δm that is linear in m_{χ^0} . This bound can be parametrized as

$$\Delta m \equiv m_{\chi^+} - m_{\chi^0} = 0.031 \left[\frac{1}{n - 4} - 0.13 \right] m_{\chi^0}. \tag{14}$$

For larger $m_{\chi^0} \sim 1$ TeV, the constraint from the T parameter becomes important and limits the value of Δm independent of m_{χ^0} . For $m_{\chi^0} \sim 5$ – 6 TeV, the unitarity limit on λ_3 becomes the strongest constraint on Δm , as shown by the dashed lines in Fig. 1.

⁴ In this table we use $g^2 = 4\pi\alpha/s_W^2$, $s_W^2 = 0.231$, and $\alpha = 1/128$.

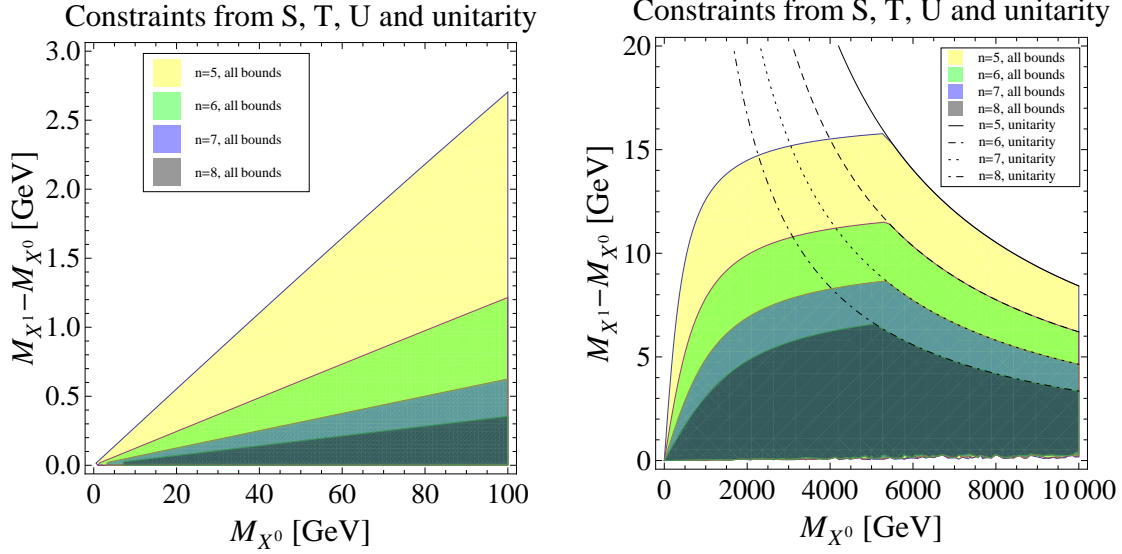


FIG. 1. The 95% confidence level constraints on $\Delta m \equiv m_{\chi^{+1}} - m_{\chi^0}$ as a function of m_{χ^0} from the S , T , and U parameters, for the scalar multiplets with $n = 5, 6, 7$, and 8 and $Y = 2T = n - 1$. Dashed lines indicate the upper limit on Δm from the unitarity bound on λ_3 . The left panel shows the low- m_{χ^0} region while the right panel extends to higher masses.

Notice that for $n \geq 6$ the mass splitting between χ^0 and the next-lightest state χ^+ is constrained to be no more than about 12 GeV; for $m_{\chi^0} \sim 100$ GeV the splitting is less than 1.5 GeV. The maximum allowed mass splitting decreases with increasing n .

C. Direct collider constraints

Scalar particle masses below about 100 GeV are constrained by $\chi^Q \chi^{Q*}$ pair production in e^+e^- collisions at the CERN Large Electron-Positron (LEP-II) collider. However, a dedicated search for the decay signatures in the models we consider here has not been made; furthermore, $\chi^Q \chi^{Q*}$ events may be difficult to detect if the mass splittings are small, leading to low-energy charged particles from the χ^Q decays.

Regardless of these difficulties, the LEP-I measurement of the Z boson invisible decay width puts a stringent constraint on $Z \rightarrow \chi^0 \chi^{0*}$ independent of the mass splittings. This leads to the requirement

$$m_{\chi^0} \gtrsim m_Z/2 \simeq 45 \text{ GeV}. \quad (15)$$

Scalar particle masses below $m_h/2 \simeq 63$ GeV are also constrained by measurements of Higgs production and decay at the CERN Large Hadron Collider (LHC). The decay width of the Higgs to $\chi^{Q*} \chi^Q$ is given by

$$\Gamma(h \rightarrow \chi^{Q*} \chi^Q) = \frac{v^2 \Lambda_Q^2}{16\pi m_h} \sqrt{1 - \frac{4m_{\chi^Q}^2}{m_h^2}}, \quad \text{for } m_{\chi^Q} \leq m_h/2, \quad (16)$$

where Λ_Q controls the $h\chi^{Q*}\chi^Q$ coupling (see Eq. (A1)).

The ATLAS experiment has recently performed a direct search for $pp \rightarrow Zh$ with $h \rightarrow$ invisible, which found a 95% confidence level upper bound $\text{BR}(h \rightarrow \text{invisible}) \leq 0.65$ [17], assuming the SM production rate for $pp \rightarrow Zh$. This can be used to constrain Λ_0 from invisible $h \rightarrow \chi^{0*}\chi^0$, as long as other decays $h \rightarrow \chi^{Q*}\chi^Q$ (with $Q \neq 0$) can be neglected. However, the electroweak precision observables tightly constrain the mass splittings among the states χ^Q , so that Higgs decays to multiple χ^Q species are generally kinematically accessible for χ^0 masses of more than a few GeV below half the Higgs mass.

Instead we take advantage of the fact that the measured Higgs signal strengths in a variety of channels at the LHC are in rough agreement with the SM predictions. Because Higgs production in our model is SM-like, this constrains the allowable decay width of the Higgs to non-SM final states. In particular, we have

$$\text{BR}(h \rightarrow \text{new}) = \frac{\Gamma_{\text{new}}}{\Gamma_{\text{tot}}^{\text{SM}} + \Gamma_{\text{new}}} = 1 - \mu_i, \quad (17)$$

where μ_i is the Higgs signal strength in any SM channel for which the Higgs decay width is the same as in the SM and $\Gamma_{\text{tot}}^{\text{SM}} \simeq 4.1$ MeV for $m_h = 125$ GeV [18]. Setting aside $h \rightarrow \gamma\gamma$, which can be modified by scalars χ^Q running in the loop (this will be addressed in Sec. V C), we take as a rough lower bound $\mu_i \gtrsim 0.35$ from Higgs decays to WW and ZZ [19] (a full fit of Higgs signal strengths in our model is beyond the scope of this paper).

We scan over λ_2 , λ_3 , and m_{χ^0} for each of the models, imposing the precision electroweak constraints on λ_3 as a function of m_{χ^0} , and compute Γ_{new} from all kinematically accessible final states. We find that the Higgs signal strength constrains $|\lambda_2| \lesssim 0.015$ for $m_{\chi^0} \leq 55$ GeV, with very little dependence on n . Closer to threshold, the bound is somewhat loosened due to kinematic suppression of the new decays; for $m_{\chi^0} = 60$ GeV, we find $|\lambda_2| \lesssim 0.05$ for $n = 5$, with a stronger constraint for higher n values due to the smaller mass splittings among the χ^Q states required by the precision electroweak constraints.

As we will show, the constraint $m_{\chi^0} \gtrsim m_Z/2$ together with cosmological considerations will be sufficient to exclude the models with $n = 6, 7$, and 8. Further investigation of the direct collider constraints on the $n = 5$ model is beyond the scope of this paper.

IV. DARK MATTER DIRECT DETECTION CONSTRAINT

The allowable relic density of $\chi^{0(*)}$ is constrained by its non-observation in direct dark matter detection experiments. In particular, the fraction of the ambient dark matter density that can be attributed to χ is bounded from above according to

$$\frac{\Omega_\chi}{\Omega_{\text{DM}}} \leq \frac{\sigma_{\text{SI}}^{\text{limit}}}{\sigma_{\text{SI}}^\chi}, \quad (18)$$

where σ_{SI}^χ is the spin-independent, per-nucleon scattering cross section for χ^0 or χ^{0*} and $\sigma_{\text{SI}}^{\text{limit}}$ is the experimental upper limit on the spin-independent dark matter scattering cross section obtained assuming the canonical ambient dark matter density. The strongest experimental upper limit currently comes from the XENON100 experiment [20]. We note that this limit will not apply to the model with $n = 5$ because in this model the relic χ^0 particles decay away on a time scale short compared to the age of the universe.

Because χ^0 is a complex scalar, it scatters off nucleons via both Z and Higgs exchange. The Z -exchange diagram yields a large scattering cross section, leading to very stringent constraints on $\Omega_\chi/\Omega_{\text{DM}}$. We compute the cross sections in the zero-velocity limit assuming equal densities of χ^0 and χ^{0*} , such that $\Omega_\chi \equiv \Omega_{\chi^0} + \Omega_{\chi^{0*}}$. We have,

$$\sigma_{\text{SI}}^{\chi^0} = \sigma_Z^{\chi^0} + \sigma_h^{\chi^0} + \sigma_{\text{int}}^{\chi^0}, \quad (19)$$

where $\sigma_{\text{int}}^{\chi^0}$ is the interference between the Z - and Higgs-exchange diagrams. For χ^{0*} we have $\sigma_{Z,h}^{\chi^{0*}} = \sigma_{Z,h}^{\chi^0}$ and $\sigma_{\text{int}}^{\chi^{0*}} = -\sigma_{\text{int}}^{\chi^0}$, so the interference term cancels in the total scattering rate for equal densities of χ^0 and χ^{0*} .

The Z -exchange cross section for scattering off a single nucleon $N = p, n$ is given by

$$\sigma_Z^\chi = \frac{(f_N^V)^2 (n-1)^2 m_{\chi^0}^2}{\pi v^2 m_Z^2} \frac{m_N^2}{(m_N + m_{\chi^0})^2}, \quad (20)$$

where $v \simeq 246$ GeV is the SM Higgs vev, m_N is the nucleon mass, and the vector couplings of the Z to the nucleon are given by the sum of the corresponding valence quark couplings,⁵

$$f_p^V = \frac{2m_Z}{v} \left(\frac{1}{4} - s_W^2 \right), \quad f_n^V = \frac{2m_Z}{v} \left(-\frac{1}{4} \right). \quad (21)$$

The axial-vector couplings do not contribute in the zero-velocity limit. Notice that σ_Z^χ becomes independent of m_{χ^0} in the large- m_{χ^0} limit, where it is of order m_N^2/v^4 . Note also that σ_Z^χ is fixed with no free parameters once m_{χ^0} and the size of the multiplet n are specified.

The h -exchange cross section for scattering off a single nucleon $N = p, n$ is given by

$$\sigma_h^\chi = \frac{(f_N^h)^2 \Lambda_0^2 v^2}{4\pi m_h^4} \frac{m_N^2}{(m_N + m_{\chi^0})^2}, \quad (22)$$

where $\Lambda_0 v$ is the $h\chi^0\chi^{0*}$ coupling defined in Eq. (5) and the Higgs-nucleon Yukawa couplings are given by [22]

$$f_p^h = \frac{m_p}{v} (0.350 \pm 0.048), \quad f_n^h = \frac{m_n}{v} (0.353 \pm 0.049). \quad (23)$$

Notice that σ_h^χ goes like $1/m_{\chi^0}^2$ in the large- m_{χ^0} limit, where it is of order $m_N^4/v^4 m_{\chi^0}^2$. The Higgs-exchange contribution is thus generically much smaller than the Z -exchange contribution. The Higgs-exchange contribution also depends on the parameter $\Lambda_0 = \lambda_2 + \lambda_3(n-1)/4$. We obtain the least stringent upper bound on $\Omega_\chi/\Omega_{\text{DM}}$ when $\Lambda_0 = 0$.

Because dark matter particles moving in the galactic halo have de Broglie wavelengths that are large compared to the size of a nucleus, the amplitudes for scattering off each nucleon add coherently. This can be accounted for by replacing f_N^V and f_N^h in Eqs. (20) and (22) above by the coherent nucleon-averaged values,

$$\begin{aligned} (f_N^V)^2 &\rightarrow (\overline{f_N^V})^2 = \frac{[Zf_p^V + (A-Z)f_n^V]^2}{A^2}, \\ (f_N^h)^2 &\rightarrow (\overline{f_N^h})^2 = \frac{[Zf_p^h + (A-Z)f_n^h]^2}{A^2} \simeq (f_p^h)^2 \simeq (f_n^h)^2, \end{aligned} \quad (24)$$

⁵ These nucleon vector couplings do not receive any QCD corrections in the limit of zero momentum transfer due to the conservation of the vector current [21].

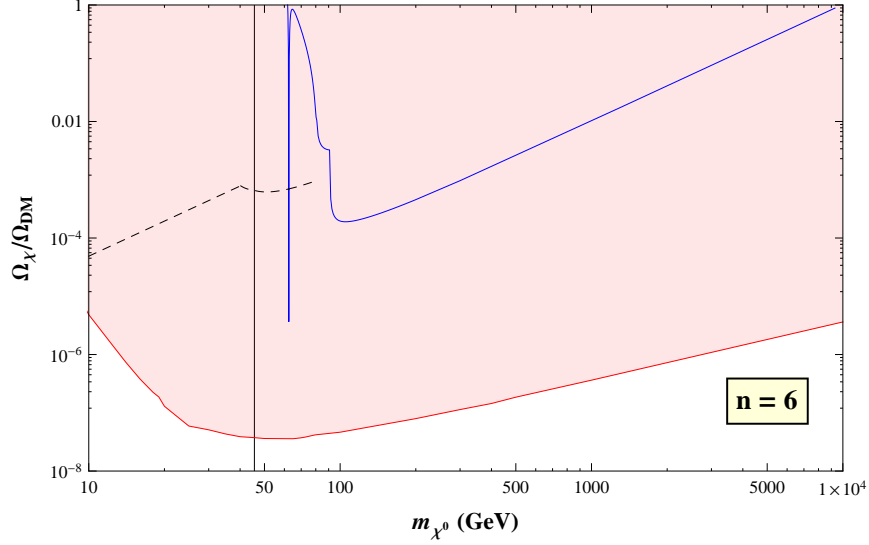


FIG. 2. The fraction $\Omega_{\chi}/\Omega_{\text{DM}}$ of the total dark matter density for the $n = 6$ model as a function of m_{χ^0} . The shaded area above the red curve is excluded by direct-detection constraints from XENON100 data [20], conservatively taking $\Lambda_0 = 0$. The solid blue curve shows the predicted relic density assuming a standard thermal history of the universe, for the parameters $\Lambda_0 = 0.01$, $\lambda_3 = -0.01$. The black dashed curve is the relic density in the case that coannihilations are maximal (see text for details). Masses below $m_Z/2$ (to the left of the vertical black line) are excluded by the LEP constraint on the invisible Z width.

where Z is the atomic number and A the atomic mass of the nucleus. For xenon, $Z = 54$ and A ranges from 124 to 136. We make a weighted average over the natural abundances of xenon isotopes [23].

The upper limit on $\Omega_{\chi}/\Omega_{\text{DM}}$ from XENON100 [20] as a function of the χ^0 mass is shown in Figs. 2 and 3 for the multiplets with $n = 6, 7$, and 8 (the limit depends on n like $1/(n-1)^2$). The shaded area bounded by the red curve is excluded. Here we have set $\Lambda_0 = 0$ in order to obtain the most conservative limit; taking $\Lambda_0 \neq 0$ has only a tiny effect on the limit.

Finally we comment on the behavior of the upper limit on $\Omega_{\chi}/\Omega_{\text{DM}}$ at large χ^0 masses. The scattering cross section $\sigma_{\text{SI}}^{\chi}$ is overwhelmingly dominated by the Z -exchange contribution, which is independent of m_{χ^0} in the large- m_{χ^0} limit. The XENON100 collaboration quotes a cross section limit for dark matter masses up to 1000 GeV. When the dark matter particle mass is large compared to the mass of the target nucleus, the energy transfer for a given target nucleus asymptotes to a constant which depends only on the velocity of the incoming dark matter particle. The experimental cross section limit then varies inversely with the ambient number density of dark matter particles, which in turn goes like the (fixed) mass density times $1/m_{\chi^0}$. Therefore, the upper bound on $\Omega_{\chi}/\Omega_{\text{DM}}$ grows linearly with m_{χ^0} for masses that are large compared to the target nucleus mass, and can be extrapolated to arbitrarily heavy masses.

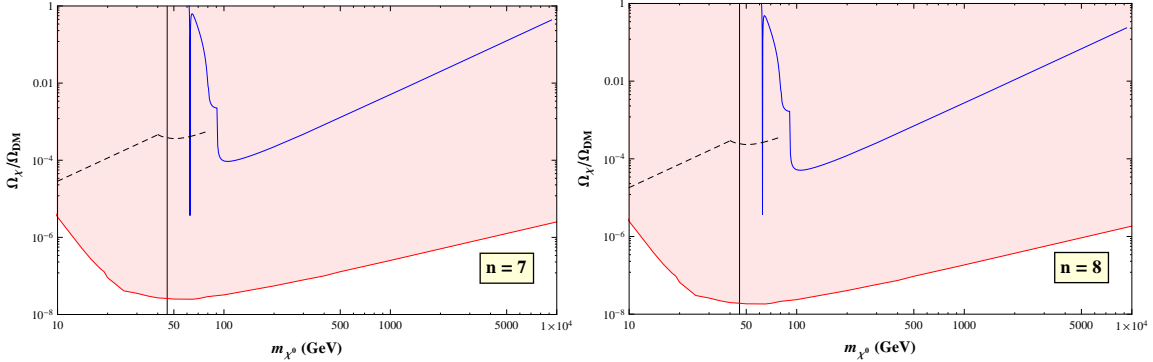


FIG. 3. The same as Fig. 2 but for $n = 7$ (left) and 8 (right).

V. THERMAL RELIC DENSITY

We now compute the thermal relic density of $\chi^0 + \chi^{0*}$ and compare it to the upper bound from direct detection found in the previous section. We assume a standard thermal history of the universe: i.e., that the temperature was high enough at one time for $\chi^{0(*)}$ to have been in thermal equilibrium, that there were no late-decaying relics that would significantly dilute the abundance of $\chi^{0(*)}$, and that there were no late-decaying relics that decayed to states in X and hence boosted the $\chi^{0(*)}$ relic abundance.

We will show that, for all allowed parameter choices, the thermal relic abundance of $\chi^{0(*)}$ is too large to be consistent with the upper bound on $\Omega_\chi/\Omega_{\text{DM}}$ from direct detection. The U(1)-preserving models with $n = 6, 7$, and 8 are thus excluded assuming a standard thermal history.

The fraction of the dark matter density that is due to χ is given in terms of the total $\chi^0\chi^{0*}$ annihilation cross section by

$$\frac{\Omega_\chi}{\Omega_{\text{DM}}} = \frac{\langle\sigma v_{\text{rel}}\rangle_{\text{std}}}{\frac{1}{2}\langle\sigma v_{\text{rel}}(\chi^0\chi^{0*} \rightarrow \text{any})\rangle}, \quad (25)$$

where v_{rel} is the relative velocity of the two colliding dark matter particles and $\langle\sigma v_{\text{rel}}\rangle_{\text{std}}$ is the “standard” annihilation cross section required to obtain the correct dark matter relic abundance, for which we use $\langle\sigma v_{\text{rel}}\rangle_{\text{std}} = 3 \times 10^{-26} \text{ cm}^3/\text{s}$ [24]. The brackets indicate an average over the velocity distribution at the time of freeze-out, which is only necessary if the annihilation cross section vanishes in the $v_{\text{rel}} \rightarrow 0$ limit. The factor of $1/2$ in the denominator accounts for the probability that, in a collision, any given χ particle meets one with the opposite U(1) charge so that an annihilation can take place. This ratio is shown by the solid blue lines in Figs. 2 and 3. We explain the ingredients in what follows.

A. Annihilation to two-body final states

A $\chi^0\chi^{0*}$ pair can annihilate to the two-body final states W^+W^- , ZZ , hh , and $f\bar{f}$. We compute the annihilation cross sections in the zero-velocity limit. Because these cross sections are all nonzero in this limit, we do not need to average over the velocity distribution.

The annihilation cross sections to two-body final states are given in the $v_{rel} \rightarrow 0$ limit by

$$\begin{aligned}
\sigma v_{rel}(\chi^0 \chi^{0*} \rightarrow W^+ W^-) &= \frac{m_W^4}{8\pi v^4} \sqrt{1 - \frac{m_W^2}{m_{\chi^0}^2}} \left[\frac{A_W^2}{m_{\chi^0}^2} \left(3 - 4 \frac{m_{\chi^0}^2}{m_W^2} + 4 \frac{m_{\chi^0}^4}{m_W^4} \right) \right. \\
&\quad \left. + 2A_W B_W \left(1 - 3 \frac{m_{\chi^0}^2}{m_W^2} + 2 \frac{m_{\chi^0}^4}{m_W^4} \right) + B_W^2 m_{\chi^0}^2 \left(1 - \frac{m_{\chi^0}^2}{m_W^2} \right)^2 \right], \\
\sigma v_{rel}(\chi^0 \chi^{0*} \rightarrow ZZ) &= \frac{m_Z^4}{16\pi v^4} \sqrt{1 - \frac{m_Z^2}{m_{\chi^0}^2}} \left[\frac{A_Z^2}{m_{\chi^0}^2} \left(3 - 4 \frac{m_{\chi^0}^2}{m_Z^2} + 4 \frac{m_{\chi^0}^4}{m_Z^4} \right) \right. \\
&\quad \left. + 2A_Z B_Z \left(1 - 3 \frac{m_{\chi^0}^2}{m_Z^2} + 2 \frac{m_{\chi^0}^4}{m_Z^4} \right) + B_Z^2 m_{\chi^0}^2 \left(1 - \frac{m_{\chi^0}^2}{m_Z^2} \right)^2 \right], \\
\sigma v_{rel}(\chi^0 \chi^{0*} \rightarrow hh) &= \frac{\Lambda_0^2}{64\pi m_{\chi^0}^2} \sqrt{1 - \frac{m_h^2}{m_{\chi^0}^2}} \left[1 + \frac{3m_h^2}{4m_{\chi^0}^2 - m_h^2} - \frac{2v^2 \Lambda_0}{2m_{\chi^0}^2 - m_h^2} \right]^2, \\
\sigma v_{rel}(\chi^0 \chi^{0*} \rightarrow f\bar{f}) &= \frac{N_c}{4\pi} \left(1 - \frac{m_f^2}{m_{\chi^0}^2} \right)^{3/2} \frac{m_f^2 \Lambda_0^2}{(4m_{\chi^0}^2 - m_f^2)^2}. \tag{26}
\end{aligned}$$

Here the coefficients in the cross sections to WW and ZZ are given by

$$\begin{aligned}
A_W &= (n-1) + \frac{v^2 \Lambda_0}{4m_{\chi^0}^2 - m_h^2}, & B_W &= \frac{4(n-1)}{m_W^2 - m_{\chi^0}^2 - m_{\chi^+}^2}, \\
A_Z &= (n-1)^2 + \frac{v^2 \Lambda_0}{4m_{\chi^0}^2 - m_h^2}, & B_Z &= -\frac{4(n-1)^2}{2m_{\chi^0}^2 - m_Z^2}. \tag{27}
\end{aligned}$$

Diagrams involving s -channel Z -exchange are zero in the low-energy limit, so that annihilation to $f\bar{f}$ proceeds only through an s -channel Higgs. We checked our analytic results by implementing the relevant couplings into CalcHEP [25].

Above threshold, $\chi^{0*} \chi^0 \rightarrow ZZ$ has the largest cross section, followed by $\chi^{0*} \chi^0 \rightarrow W^+ W^-$, which is smaller by about a factor of 20 for $n = 6$. Annihilation rates to hh and $t\bar{t}$ are much smaller, as can be seen by the fact that their kinematic thresholds are not even visible in Figs. 2 and 3. The latter two processes are controlled by the coupling Λ_0 ; we took the sample value $\Lambda_0 = 0.01$ in Figs. 2 and 3. As we will see in Sec. V C, significantly larger values of Λ_0 are constrained by the measured rate for $h \rightarrow \gamma\gamma$. Λ_0 also contributes to the annihilations to WW and ZZ through the A_W and A_Z coefficients; its effect is numerically small and falls with increasing m_{χ^0} . We also took the sample value $\lambda_3 = -0.01$; λ_3 has a tiny effect on the annihilation cross section to WW through the $\chi^0 - \chi^+$ mass splitting. Overall, the total annihilation cross section above the WW threshold depends very weakly on Λ_0 and λ_3 , and is instead controlled almost entirely by n and m_{χ^0} .

The cross sections for annihilation to WW , ZZ , and hh fall like $1/m_{\chi^0}^2$ at large m_{χ^0} , while the cross section to $f\bar{f}$ falls like $1/m_{\chi^0}^4$. This leads to the growth of $\Omega_\chi/\Omega_{\text{DM}}$ proportional to $m_{\chi^0}^2$ for large m_{χ^0} shown in Figs. 2 and 3. As we saw in Sec. IV, the upper bound on $\Omega_\chi/\Omega_{\text{DM}}$ from direct detection grows only linearly with m_{χ^0} . Increasing m_{χ^0} thus leads only to more severe conflict between the relic abundance and the direct-detection limit.

We finally comment on the possibility that attractive electroweak interactions between χ^0 and χ^{0*} form bound states that increase the annihilation cross section for $m_{\chi^0} \gg m_W$, an effect known

as Sommerfeld enhancement [26]. This effect was studied in Ref. [27] for a real scalar 7-plet with hypercharge zero, which found an increase in the mass at which the dark matter candidate obtained the correct relic density by about a factor of 3 (to about 25 TeV), corresponding to about an order of magnitude enhancement of the annihilation cross section during freeze-out. However, for our models, the direct-detection constraint is 10^5 – 10^6 times stronger than the perturbative relic density at large $m_{\chi^0} \gtrsim 1$ TeV. We expect that an enhancement of the annihilation cross section that is sufficiently large to affect our exclusion would be extremely difficult to obtain.

B. Annihilation to off-shell WW below threshold

Below the WW threshold, the largest two-body annihilation process is $\chi^{0*}\chi^0 \rightarrow b\bar{b}$, which has a small cross section. Annihilation to off-shell WW can be significantly larger. We compute the annihilation cross section to off-shell WW by generating $\chi^{0*}\chi^0 \rightarrow e^+\nu_e e^-\bar{\nu}_e$ using CalcHEP [25] and then multiplying by $[1/\text{BR}(W \rightarrow e\nu)]^2 = 81$ at tree level. We include $b\bar{b}$ and off-shell WW in the blue solid curves in Figs. 2 and 3 for $m_{\chi^0} < m_W$. We again take $\Lambda_0 = 0.01$ and $\lambda_3 = -0.01$. Annihilations to off-shell ZZ could also be included; however, their contribution is very small compared to off-shell WW because the Z bosons are further off shell for a given m_{χ^0} .

C. Resonant annihilation through the Higgs pole

The most interesting feature in the annihilation cross section below the WW threshold is the Higgs pole at $m_{\chi^0} = m_h/2$. The possibility that this resonant annihilation may suppress the X relic density enough to evade the direct-detection constraints is excluded by a combination of constraints from the oblique parameters and the observed rate for $pp \rightarrow h \rightarrow \gamma\gamma$ from the LHC [28].

The $\chi^0\chi^{0*} \rightarrow h \rightarrow b\bar{b}$ annihilation cross section near the Higgs resonance is obtained from the last line of Eq. (26) by making the replacement in the denominator,

$$(4m_{\chi^0}^2 - m_h^2)^2 \rightarrow (4m_{\chi^0}^2 - m_h^2)^2 + m_h^2\Gamma_h^2. \quad (28)$$

Here Γ_h is the total decay width of the SM Higgs boson; the contribution from $b\bar{b}$ final states is given at tree level by [29]

$$\Gamma(h \rightarrow b\bar{b}) = \frac{N_c m_b^2 m_h}{8\pi v^2} \left(1 - \frac{4m_b^2}{m_h^2}\right)^{3/2}, \quad (29)$$

where $N_c = 3$ is the number of colors.

Note that we can capture the effects of higher-order corrections and additional final states on $\sigma v_{rel}(\chi^0\chi^{0*} \rightarrow h \rightarrow \text{any})$ near the Higgs resonance simply by choosing the value of m_b to yield the correct total SM Higgs width, $\Gamma_h = 4.07 \pm 0.16$ MeV [18] for $m_h = 125$ GeV. We obtain this width from the tree-level formula above when $m_b = 4.08$ GeV. Using this value of m_b , we compute $\Omega_\chi/\Omega_{\text{DM}}$ in the vicinity of the Higgs resonance using the tree-level $\chi^0\chi^{0*} \rightarrow b\bar{b}$ cross section and $h \rightarrow b\bar{b}$ partial width. The result is shown in Fig. 4 for various values of Λ_0 .⁶

⁶ When specified in terms of Λ_0 , $\sigma v_{rel}(\chi^0\chi^{0*} \rightarrow b\bar{b})$ is independent of n .

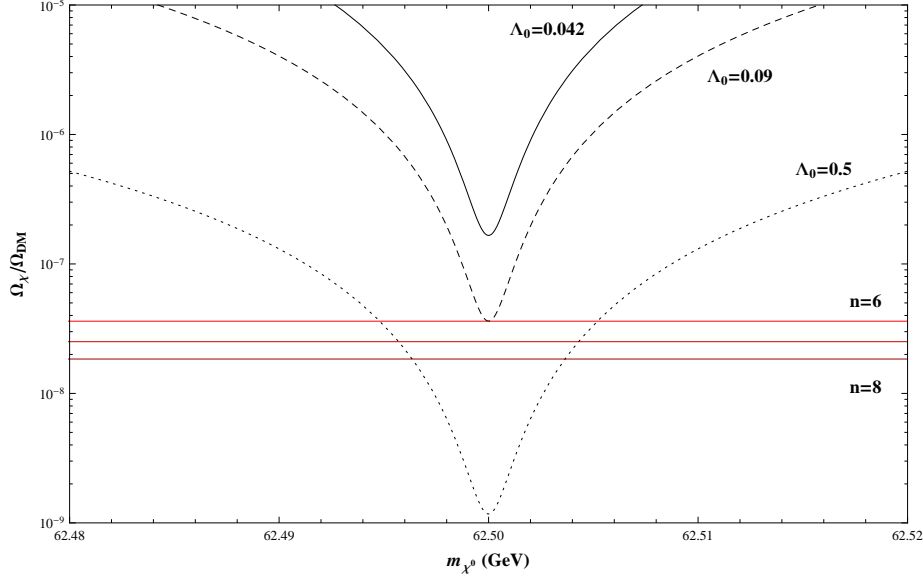


FIG. 4. Fractional relic density $\Omega_\chi/\Omega_{\text{DM}}$ for $m_{\chi^0} \simeq m_h/2$ from $\chi^0 \chi^{0*} \rightarrow b\bar{b}$ annihilation, for various values of Λ_0 (solid, dashed, and dotted black curves). Also shown are the upper limits on $\Omega_\chi/\Omega_{\text{DM}}$ from direct detection for (top to bottom) $n = 6, 7$, and 8 (red horizontal lines).

n	λ_3^{lim}
5	-1.4×10^{-2}
6	-6.0×10^{-3}
7	-3.3×10^{-3}
8	-2.0×10^{-3}

TABLE II. The 95% confidence level lower limit on λ_3 from the S , T , and U parameter constraints as a function of the size of the multiplet, for $m_{\chi^0} = m_h/2 = 62.5$ GeV.

The cross section for $\chi^0 \chi^{0*} \rightarrow b\bar{b}$ is proportional to Λ_0^2 , which in turn depends on λ_2 and λ_3 . These couplings also control the one-loop contribution of χ^Q to the Higgs decay to two photons. Setting $m_{\chi^0} = m_h/2$, the S , T and U parameters put an upper bound on $|\lambda_3|$, as summarized in Table II ($\lambda_3 < 0$ is required in order for χ^0 to be the lightest member of the multiplet). For λ_3 within the allowed range, we compute the partial width $\Gamma(h \rightarrow \gamma\gamma)$ as a function of λ_2 , leading to a constraint on Λ_0 . The contributions of the charged χ^Q states to $\Gamma(h \rightarrow \gamma\gamma)$ are summarized in Appendix C. This partial width normalized to its SM value is shown as a function of Λ_0 in Fig. 5 for the two extreme cases, $\lambda_3 = 0$ and the limiting value allowed by the S , T , and U parameter constraints.

We see that increasing $|\Lambda_0|$ quickly drives $\Gamma(h \rightarrow \gamma\gamma)$ to unacceptably large values. In particular, $|\Lambda_0| \gtrsim 0.09$ – which is required to evade the direct-detection limit for the $n = 6$ model – is ruled out

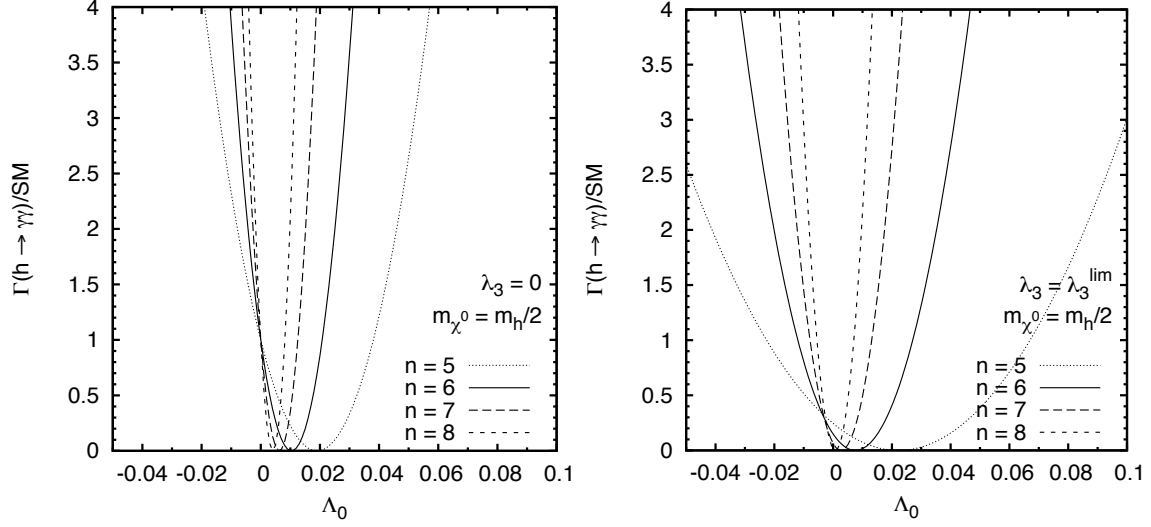


FIG. 5. The partial width for $h \rightarrow \gamma\gamma$ normalized to its SM value as a function of Λ_0 , for $m_{\chi^0} = m_h/2 = 62.5$ GeV and $\lambda_3 = 0$ (left) and the limiting (minimum) value allowed by the S , T , and U parameter constraints as given in Table II (right).

by the LHC measurement of the signal strength for $pp \rightarrow h \rightarrow \gamma\gamma$.⁷ Allowing a very generous factor of three enhancement over the SM prediction (already excluded at more than 2σ by both ATLAS and CMS [28]) requires $|\Lambda_0| < 0.042$ for $n = 6$; the limit becomes more stringent for larger n . After applying these constraints, we see that resonant annihilation through the Higgs pole cannot suppress $\Omega_\chi/\Omega_{\text{DM}}$ enough to allow us to evade the direct-detection limits.

D. Coannihilations

We finally consider the possibility that the mass splittings among the states χ^Q are very small, as is favored by the oblique parameter constraints for low χ^0 masses. In this case, all members of the multiplet can be present in the thermal bath during freeze-out. This opens the possibility of annihilations involving the electrically charged states χ^Q to $\gamma\gamma$, $Z\gamma$, and $W^\pm\gamma$ final states,⁸ which are on shell below the WW threshold. Such electroweak-strength annihilation cross sections to two-body final states can easily dominate over those to three-body final states and the bottom-Yukawa-suppressed annihilation cross section to $b\bar{b}$.

We evaluate the potential impact of such coannihilations by considering the extreme case in which all states $\chi^{Q(*)}$ are present with equal abundances during freeze-out. Two conditions are required: the mass splittings must be very small so that the equilibrium thermal abundances of each species are equal, and the quartic couplings multiplying operators $\mathcal{O}(X^4)$ must be large enough to maintain

⁷ In the models considered here, the Higgs couplings are identical to those in the SM except for the contributions to the loop-induced $h\gamma\gamma$ and $h\gamma Z$ couplings from loops of charged scalars. Because the decays to $\gamma\gamma$ and γZ contribute only a tiny fraction of the Higgs total width, the LHC Higgs signal strength in the $\gamma\gamma$ channel is given to a very good approximation by $\mu \equiv \sigma(pp \rightarrow h \rightarrow \gamma\gamma)/\sigma_{\text{SM}}(pp \rightarrow h \rightarrow \gamma\gamma) \simeq \Gamma(h \rightarrow \gamma\gamma)/\Gamma_{\text{SM}}(h \rightarrow \gamma\gamma)$.

⁸ The cross section for $\chi^Q\chi^{Q*} \rightarrow h\gamma$ vanishes in the zero-velocity limit.

equal abundances of states with each charge, even though the annihilation cross section to SM states is different for states with different charge. For larger mass splittings, coannihilations become less important, and the situation relaxes to our original analysis.

In the limit of equal abundances of all states $\chi^{Q(*)}$, the fraction of the dark matter density due to χ is given in terms of the annihilation cross sections by

$$\frac{\Omega_\chi}{\Omega_{\text{DM}}} = \frac{\langle \sigma v_{\text{rel}} \rangle_{\text{std}}}{\frac{1}{2} \frac{1}{n^2} \sum_{Q_1, Q_2 \geq 0} \langle \sigma v_{\text{rel}} (\chi^{Q_1} \chi^{Q_2*} \rightarrow \text{any}) \rangle}. \quad (30)$$

Note in particular the new factor $1/n^2$ in the denominator, which represents the average over initial charge states for a multiplet of size n . The sum runs over all initial charge combinations; only the combinations with $Q_1 - Q_2 = 0$ and ± 1 contribute below the WW threshold. We include annihilations to the two-body final states $\gamma\gamma$, $Z\gamma$, $W^\pm\gamma$, and $b\bar{b}$. Cross section formulas are given in Appendix D. The cross sections for the first three processes are independent of Λ_0 and depend on λ_3 only through the masses m_{χ^Q} . For the scalar couplings we set $\Lambda_0 = 0.01$ as usual but we now take $\lambda_3 = 0$, corresponding to degenerate masses for all χ^Q .

The resulting relic abundance of χ in the full coannihilation case is shown by the black dashed lines in Figs. 2 and 3. The relic abundance is dramatically reduced compared to that obtained considering only $\chi^0\chi^{0*}$ annihilations. However, coannihilations still do not allow us to evade the direct-detection limits: the relic density of χ remains about four orders of magnitude above the direct-detection exclusion bound for $m_Z/2 \leq m_{\chi^0} \leq m_W$.

VI. CONCLUSIONS

In this paper we studied the class of models in which the SM Higgs sector is extended by a single large complex scalar multiplet in such a way that the Higgs potential preserves an accidental⁹ global $U(1)$ symmetry at the renormalizable level. The accidental $U(1)$ symmetry is present when $n = 2T + 1 \geq 5$. Perturbative unitarity of weak-interaction scattering amplitudes involving the large multiplet excludes multiplets with $n > 8$. We choose the hypercharge to be $Y = 2T$ so that the lightest member of the large multiplet can be electrically neutral.

We showed that the models with $n = 6, 7$, or 8 are excluded by the incompatibility of the standard thermal freeze-out relic density with the dark matter direct-detection cross section limit, assuming a standard thermal history of the universe. The model with $n = 5$ evades the direct-detection constraint because its lightest state can decay via a Planck-suppressed dimension-5 operator during the first few days to few years after the big bang.

This exclusion can be evaded if the model is modified in such a way as to break the global $U(1)$ symmetry. One approach is to add one or more additional, smaller scalar multiplets in such a way that the accidental global symmetry is eliminated. This induces effective higher-dimensional operators involving the SM Higgs field and the large multiplet X that break the global $U(1)$. Such operators typically also induce a vev for X and mixing between the states of X and the SM Higgs doublet. Models of this type involving a large multiplet with $n = 7$ and $Y = 4$ (whose vev preserves $\rho = 1$ at tree level [29, 30]) have recently been discussed in Ref. [9].

A second approach is to arrange the model in such a way that the global $U(1)$ is broken down to Z_2 . In this case, the real and imaginary components of the neutral member of X can be arranged

⁹ We do not consider models where the additional $U(1)$ symmetry is imposed by hand, such as the $Y = 0$ case outlined in Ref. [11].

to have different masses, so that the Z -mediated direct-detection scattering process $\chi^{0,r}N \rightarrow \chi^{0,i}N$ is kinematically forbidden. The h -mediated process $\chi^{0,r}N \rightarrow \chi^{0,r}N$ has a much smaller cross section and remains experimentally viable. Such a model can be constructed for a large multiplet with $n = 6$ or $n = 8$ if its hypercharge is chosen as $Y = 1$. Then the U(1)-breaking operator $(\Phi^\dagger \tau^a \tilde{\Phi})(\tilde{X}^\dagger T^a X)$ appears in the scalar potential, where $\tilde{\Phi}$ and \tilde{X} denote the conjugate multiplets. We will address such models in Ref. [13].

ACKNOWLEDGMENTS

We thank Thomas Grégoire for helpful discussions on the unitarity constraints. This work was supported by the Natural Sciences and Engineering Research Council of Canada.

Appendix A: Feynman rules

We summarize the Feynman rules for the couplings of χ states to gauge and Higgs bosons. The following are for all particles and momenta incoming. We take $Q \geq 0$ and denote the antiparticle of χ^Q as χ^{Q*} .

Couplings to one or two Higgs bosons are as follows:

$$\begin{aligned}\chi^{Q*}\chi^Q h &= -iv \left[\lambda_2 - \frac{1}{2}\lambda_3 \left(Q - \frac{n-1}{2} \right) \right] = -iv\Lambda_Q \\ \chi^{Q*}\chi^Q hh &= -i \left[\lambda_2 - \frac{1}{2}\lambda_3 \left(Q - \frac{n-1}{2} \right) \right] = -i\Lambda_Q.\end{aligned}\tag{A1}$$

Couplings to two gauge bosons are as follows:

$$\begin{aligned}\chi^{Q*}\chi^Q W_\mu^+ W_\nu^- &= \frac{ie^2}{s_W^2} \left[(2Q+1)\frac{(n-1)}{2} - Q^2 \right] g_{\mu\nu} \\ \chi^{(Q+2)*}\chi^Q W_\mu^+ W_\nu^+ &= \frac{ie^2}{s_W^2} \sqrt{(Q+2)(n-2-Q)(Q+1)(n-1-Q)} g_{\mu\nu} = \chi^{Q*}\chi^{Q+2} W_\mu^- W_\nu^- \\ \chi^{Q*}\chi^Q A_\mu A_\nu &= 2ie^2 Q^2 g_{\mu\nu} \\ \chi^{Q*}\chi^Q Z_\mu Z_\nu &= \frac{2ie^2}{s_W^2 c_W^2} \left[c_W^2 Q - \frac{n-1}{2} \right]^2 g_{\mu\nu} \\ \chi^{Q*}\chi^{Q+1} W_\mu^- A_\nu &= \frac{ie^2}{s_W} \sqrt{\frac{(Q+1)(n-1-Q)}{2}} (1+2Q) g_{\mu\nu} = \chi^{(Q+1)*}\chi^Q W_\mu^+ A_\nu \\ \chi^{Q*}\chi^{Q+1} W_\mu^- Z_\nu &= \frac{ie^2}{s_W^2 c_W} \sqrt{\frac{(Q+1)(n-1-Q)}{2}} [(1+2Q)c_W^2 - n+1] g_{\mu\nu} = \chi^{(Q+1)*}\chi^Q W_\mu^+ Z_\nu \\ \chi^{Q*}\chi^Q Z_\mu A_\nu &= \frac{2ie^2 Q}{s_W c_W} \left[c_W^2 Q - \frac{n-1}{2} \right] g_{\mu\nu}.\end{aligned}\tag{A2}$$

Couplings to one gauge boson are as follows:

$$\begin{aligned}
\chi^{Q*}(p)\chi^{Q+1}(k)W_\mu^- &= -\frac{ie}{s_W}\sqrt{\frac{(Q+1)(n-1-Q)}{2}}(k-p)_\mu = \chi^{(Q+1)*}(p)\chi^Q(k)W_\mu^+ \\
\chi^{Q*}(p)\chi^Q(k)A_\mu &= -ieQ(k-p)_\mu \\
\chi^{Q*}(p)\chi^Q(k)Z_\mu &= -\frac{ie}{s_W c_W}\left[c_W^2 Q - \frac{n-1}{2}\right](k-p)_\mu.
\end{aligned} \tag{A3}$$

Appendix B: Contributions to the oblique parameters from a scalar electroweak multiplet

For a multiplet of hypercharge Y and size $n = 2T + 1$, the contribution to the S parameter is given by [15]

$$S = \frac{4s_W^2 c_W^2}{\alpha} \left[\Pi'_{ZZ}(0) - \frac{c_W^2 - s_W^2}{c_W s_W} \Pi'_{Z\gamma}(0) - \Pi'_{\gamma\gamma}(0) \right] = -\frac{Y}{6\pi} \sum_{i=0}^{n-1} T_i^3 \log(m_i^2), \tag{B1}$$

where m_i and T_i^3 denote the mass and third component of isospin of the complex scalar mass eigenstate χ_i .¹⁰

The contribution to the T parameter can be similarly represented as [15]

$$\begin{aligned}
T &= \frac{1}{\alpha} \left[\frac{\Pi_{WW}(0)}{m_W^2} - \frac{\Pi_{ZZ}(0)}{m_Z^2} \right] \\
&= \frac{1}{4\pi m_Z^2 s_W^2 c_W^2} \left[\sum_{i=0}^{n-1} m_i^2 \log(m_i^2) [T(T+1) - (T_i^3)^2] \right. \\
&\quad \left. - \sum_{i=0}^{n-2} (T - T_i^3)(T + T_i^3 + 1) f_2(m_i, m_{i+1}) \right],
\end{aligned} \tag{B2}$$

where

$$f_2(m_1, m_2) = \int_0^1 dx [xm_1^2 + (1-x)m_2^2] \log [xm_1^2 + (1-x)m_2^2]. \tag{B3}$$

Finally, the contribution to the U parameter is [15]

$$\begin{aligned}
U &= \frac{4s_W^2}{\alpha} [\Pi'_{WW}(0) - c_W^2 \Pi'_{ZZ}(0) - 2s_W c_W \Pi'_{Z\gamma}(0) - s_W^2 \Pi'_{\gamma\gamma}(0)] \\
&= \frac{1}{\pi} \left[\sum_{i=0}^{n-2} (T - T_i^3)(T + T_i^3 + 1) f_1(m_i, m_{i+1}) - \frac{1}{3} \sum_{i=0}^{n-1} (T_i^3)^2 \log(m_i^2) \right],
\end{aligned} \tag{B4}$$

where

$$f_1(m_1, m_2) = \int_0^1 dx x(1-x) \log [xm_1^2 + (1-x)m_2^2]. \tag{B5}$$

¹⁰ Note that we use the convention $Q = T^3 + Y/2$ and as such Y in the results of [15] must be replaced by $Y/2$.

We constrain these contributions to oblique parameters using a χ^2 variable including the correlations in the measured S , T , and U values,

$$\chi^2 = \sum_{i,j} (\mathcal{O}_i - \mathcal{O}_i^{\text{exp}})(\mathcal{O}_j - \mathcal{O}_j^{\text{exp}})[\sigma^2]_{ij}^{-1}, \quad (\text{B6})$$

where \mathcal{O}_i is the i th observable and $[\sigma^2]_{ij}^{-1}$ is the inverse of the matrix of uncertainties,

$$[\sigma^2]_{ij} = \Delta \mathcal{O}_i \Delta \mathcal{O}_j \rho_{ij}, \quad (\text{B7})$$

where ρ_{ij} are the relative correlations (note $\rho_{ii} = 1$). For the three-observable case of interest, we can invert the matrix σ^2 explicitly and write

$$\begin{aligned} \chi^2 = & \frac{1}{(1 - \rho_{ST}^2 - \rho_{TU}^2 - \rho_{SU}^2 + 2\rho_{ST}\rho_{TU}\rho_{SU})} \left[\frac{(1 - \rho_{TU}^2)(S - S_{\text{exp}})^2}{(\Delta S_{\text{exp}})^2} + \frac{(1 - \rho_{SU}^2)(T - T_{\text{exp}})^2}{(\Delta T_{\text{exp}})^2} \right. \\ & + \frac{(1 - \rho_{ST}^2)(U - U_{\text{exp}})^2}{(\Delta U_{\text{exp}})^2} - 2(\rho_{ST} - \rho_{TU}\rho_{SU}) \frac{(S - S_{\text{exp}})(T - T_{\text{exp}})}{\Delta S_{\text{exp}} \Delta T_{\text{exp}}} \\ & \left. - 2(\rho_{TU} - \rho_{ST}\rho_{SU}) \frac{(T - T_{\text{exp}})(U - U_{\text{exp}})}{\Delta T_{\text{exp}} \Delta U_{\text{exp}}} - 2(\rho_{SU} - \rho_{TU}\rho_{ST}) \frac{(S - S_{\text{exp}})(U - U_{\text{exp}})}{\Delta S_{\text{exp}} \Delta U_{\text{exp}}} \right] \quad (\text{B8}) \end{aligned}$$

Here S_{exp} , T_{exp} , and U_{exp} are the experimental central values, ΔS_{exp} , ΔT_{exp} and ΔU_{exp} are their 1σ experimental uncertainties, ρ_{ST} , ρ_{SU} , and ρ_{TU} are their relative correlations, and S , T , and U are the contributions from the scalar multiplet computed using the formulas above.

Appendix C: Contribution to $h \rightarrow \gamma\gamma$

The experimental observation of $pp \rightarrow h \rightarrow \gamma\gamma$ with a rate close to its SM value allows us to constrain the strength of the $\chi^0 \chi^{0*} h$ coupling in the Higgs pole annihilation region, $m_{\chi^0} \sim m_h/2$. The charged members of the X multiplet contribute to the loop-induced $h \rightarrow \gamma\gamma$ partial width [29],

$$\Gamma(h \rightarrow \gamma\gamma) = \frac{\alpha^2 g^2}{1024 \pi^3} \frac{m_h^3}{m_W^2} \left| \sum_i N_{ci} Q_i^2 F_i(\tau) \right|^2, \quad (\text{C1})$$

where i runs over charged particles of spin 1, 1/2, and 0, Q is the electric charge in units of e , N_{ci} is the color multiplicity and the functions $F_i(\tau)$ depend on the particle's spin,

$$\begin{aligned} F_1 &= 2 + 3\tau + 3\tau(2 - \tau)f(\tau) \\ F_{1/2} &= -2\tau[1 + (1 - \tau)f(\tau)] \\ F_0 &= \beta\tau[1 - \tau f(\tau)]. \end{aligned} \quad (\text{C2})$$

Here $\tau = 4m_i^2/m_h^2$, and the function $f(\tau)$ is given by

$$f(\tau) = \begin{cases} \left[\arcsin\left(\sqrt{\frac{1}{\tau}}\right) \right]^2 & \text{if } \tau \geq 1 \\ -\frac{1}{4} \left[\ln\left(\frac{\eta_+}{\eta_-} - i\pi\right) \right]^2 & \text{if } \tau < 1, \end{cases} \quad (\text{C3})$$

where we have defined $\eta_{\pm} = 1 \pm \sqrt{1 - \tau}$.

For the scalars, the coupling to the Higgs is parameterized by

$$\beta_i = \frac{m_i^2 \text{ due to Higgs}}{m_i^2} = \frac{v^2(\lambda_2/2 - \lambda_3 T_i^3/4)}{M^2 + v^2(\lambda_2/2 - \lambda_3 T_i^3/4)} = \frac{v^2 \Lambda_Q/2}{M^2 + v^2 \Lambda_Q/2}, \quad (\text{C4})$$

where T_i^3 is the third component of isospin of the scalar χ_i and Λ_Q is defined in Eq. (A1).

Appendix D: Cross sections for coannihilations

The cross sections for annihilations of charged χ states into $\gamma\gamma$, $Z\gamma$, $W^{\pm}\gamma$, and $f\bar{f}$ relevant for coannihilations below the WW threshold are given by

$$\begin{aligned} \sigma v_{rel}(\chi^{Q*} \chi^Q \rightarrow \gamma\gamma) &= \frac{e^4 Q^4}{8\pi m_{\chi^Q}^2} \\ \sigma v_{rel}(\chi^{Q*} \chi^Q \rightarrow Z\gamma) &= \frac{e^4 Q^2}{4\pi m_{\chi^Q}^2 s_W^2 c_W^2} \left[Q c_W^2 - \frac{(n-1)}{2} \right]^2 \left(1 - \frac{m_Z^2}{4m_{\chi^Q}^2} \right) \\ \sigma v_{rel}(\chi^{Q*} \chi^{Q+1} \rightarrow W^+\gamma) &= \frac{e^4 (Q+1)(n-1-Q)(2Q+1)^2}{32\pi m_{\chi^Q} m_{\chi^{Q+1}} s_W^2} \left(1 - \frac{m_W^2}{(m_{\chi^Q} + m_{\chi^{Q+1}})^2} \right) \\ &= \sigma v_{rel}(\chi^{(Q+1)*} \chi^Q \rightarrow W^-\gamma) \\ \sigma v_{rel}(\chi^{Q*} \chi^Q \rightarrow f\bar{f}) &= \frac{N_c}{4\pi} \left(1 - \frac{m_f^2}{m_{\chi^Q}^2} \right)^{3/2} \frac{m_f^2 \Lambda_Q^2}{(4m_{\chi^Q}^2 - m_h^2)^2}, \end{aligned} \quad (\text{D1})$$

where Λ_Q was defined in Eq. (A1).

-
- [1] P. Fayet, Phys. Lett. B **64**, 159 (1976); Phys. Lett. B **69**, 489 (1977); Phys. Lett. B **84**, 421 (1979); G. R. Farrar and P. Fayet, Phys. Lett. B **76**, 575 (1978).
 - [2] N. Arkani-Hamed, A. G. Cohen and H. Georgi, Phys. Lett. B **513**, 232 (2001) [hep-ph/0105239]; N. Arkani-Hamed, A. G. Cohen, E. Katz, A. E. Nelson, T. Gregoire and J. G. Wacker, JHEP **0208**, 021 (2002) [hep-ph/0206020]; N. Arkani-Hamed, A. G. Cohen, E. Katz and A. E. Nelson, JHEP **0207**, 034 (2002) [hep-ph/0206021]; M. Schmaltz and D. Tucker-Smith, Ann. Rev. Nucl. Part. Sci. **55**, 229 (2005) [hep-ph/0502182].
 - [3] M. Cirelli, N. Fornengo and A. Strumia, Nucl. Phys. B **753**, 178 (2006) [hep-ph/0512090].
 - [4] M. Cirelli and A. Strumia, New J. Phys. **11**, 105005 (2009) [arXiv:0903.3381 [hep-ph]].
 - [5] Y. Cai, W. Chao and S. Yang, arXiv:1208.3949 [hep-ph].
 - [6] K. S. Babu, S. Nandi and Z. Tavartkiladze, Phys. Rev. D **80**, 071702 (2009) [arXiv:0905.2710 [hep-ph]].
 - [7] I. Picek and B. Radovic, Phys. Lett. B **687**, 338 (2010) [arXiv:0911.1374 [hep-ph]]; K. Kumericki, I. Picek and B. Radovic, Phys. Rev. D **84**, 093002 (2011) [arXiv:1106.1069 [hep-ph]].
 - [8] B. Ren, K. Tsumura and X.-G. He, Phys. Rev. D **84**, 073004 (2011) [arXiv:1107.5879 [hep-ph]].
 - [9] J. Hisano and K. Tsumura, arXiv:1301.6455 [hep-ph]; S. Kanemura, M. Kikuchi and K. Yagyu, arXiv:1301.7303 [hep-ph].
 - [10] K. Hally, H. E. Logan and T. Pilkington, Phys. Rev. D **85**, 095017 (2012) [arXiv:1202.5073 [hep-ph]].
 - [11] J. Kopp, E. T. Neil, R. Primulando and J. Zupan, Phys. Dark. Univ. **2**, 22 (2013) [arXiv:1301.1683 [hep-ph]].

- [12] G. Aad *et al.* [ATLAS Collaboration], arXiv:1301.5272 [hep-ex].
- [13] K. Earl, K. Hartling, H. E. Logan and T. Pilkington, in preparation.
- [14] M. E. Peskin and T. Takeuchi, Phys. Rev. Lett. **65**, 964 (1990); Phys. Rev. D **46**, 381 (1992).
- [15] L. Lavoura and L.-F. Li, Phys. Rev. D **49**, 1409 (1994) [hep-ph/9309262]; H.-H. Zhang, W.-B. Yan and X.-S. Li, Mod. Phys. Lett. A **23**, 637 (2008) [hep-ph/0612059].
- [16] M. Baak, M. Goebel, J. Haller, A. Hoecker, D. Kennedy, R. Kogler, K. Moenig and M. Schott *et al.*, Eur. Phys. J. C **72**, 2205 (2012) [arXiv:1209.2716 [hep-ph]].
- [17] ATLAS Collaboration, ATLAS-CONF-2013-011 (2013), available from <http://cdsweb.cern.ch>.
- [18] S. Dittmaier, S. Dittmaier, C. Mariotti, G. Passarino, R. Tanaka, S. Alekhin, J. Alwall and E. A. Bagnaschi *et al.*, arXiv:1201.3084 [hep-ph].
- [19] ATLAS Collaboration, ATLAS-CONF-2013-034 (2013); CMS Collaboration, CMS-PAS-HIG-13-005 (2013), available from <http://cdsweb.cern.ch>.
- [20] E. Aprile *et al.* [XENON100 Collaboration], Phys. Rev. Lett. **109**, 181301 (2012) [arXiv:1207.5988 [astro-ph.CO]].
- [21] S. S. Gershtein and Y. B. Zeldovich, Zh. Eksp. Teor. Fiz. **29**, 698 (1955); R. P. Feynman and M. Gell-Mann, Phys. Rev. **109**, 193 (1958); for a review see C. S. Wu, Rev. Mod. Phys. **36**, 618 (1964).
- [22] J. R. Ellis, A. Ferstl and K. A. Olive, Phys. Lett. B **481**, 304 (2000) [hep-ph/0001005].
- [23] K. S. Krane, *Introductory Nuclear Physics* (Wiley, New York, 1988).
- [24] G. Steigman, B. Dasgupta and J. F. Beacom, Phys. Rev. D **86**, 023506 (2012) [arXiv:1204.3622 [hep-ph]].
- [25] A. Belyaev, N. D. Christensen and A. Pukhov, arXiv:1207.6082 [hep-ph].
- [26] J. Hisano, S. Matsumoto, M. Nagai, O. Saito and M. Senami, Phys. Lett. B **646**, 34 (2007) [hep-ph/0610249].
- [27] M. Cirelli, A. Strumia and M. Tamburini, Nucl. Phys. B **787**, 152 (2007) [arXiv:0706.4071 [hep-ph]].
- [28] ATLAS Collaboration, ATLAS-CONF-2012-091 (2012); CMS Collaboration, CMS-PAS-HIG-12-015 (2012), available from <http://cdsweb.cern.ch>.
- [29] J. F. Gunion, H. E. Haber, G. L. Kane, and S. Dawson, *The Higgs Hunter's Guide* (Westview, Boulder, 2000).
- [30] H.-S. Tsao, in *Proceedings of the 1980 Guangzhou Conference on Theoretical Particle Physics*, ed. H. Ning and T. Hung-yuan (Science Press, Beijing, 1980), p. 1240.